Progress In Electromagnetics Research C, Vol. 114, 129–142, 2021

Design of a Broadband Low-Profile Dual-Polarized Antenna for 5G Base Station

Wenkai Xu* **and Zhenhong Fan**

Abstract—In this paper, a novel low-profile and dual-polarized antenna is presented. The antenna is composed of two pairs of rhombic dipoles excited by two orthogonal baluns. The broadband characteristic is achieved by introducing a metal ring under the rhombic dipole, and the radiation pattern beam widths are also improved. Based on the antenna unit, a 2-element antenna array is designed, fabricated, and measured. The relative bandwidth (standing wave less than 1.5) of the antenna is 45.1%, and the port isolation is greater than 27 dB, whereas the cross-polarization level maintains lower than 16 dB in the frequency band of 2.4–3.8 GHz. The measured results are in good agreement with the simulated ones. This proposed antenna also has low profile characteristics, and the profile height is 20.8 mm, which is less than one quarter of the wavelength (24.2 mm) of the central frequency point ($f = 3.1$ GHz).

1. INTRODUCTION

Dual polarization micro base station antenna plays an important role in 5G communication system, which can realize polarization diversity with low cost and high space utilization. It has been widely concerned by academia and industry [1–4]. In order to meet the needs of 5G communication system, various forms of dual polarized antennas have been proposed. Most of these antennas are arranged in the form of orthogonal dipoles at the front of the metal reflector [5–9]. However, due to the reflection phase of the reflector, the profile of these antennas is about 0.25 wavelength. In order to solve the problem of 180° reflection phase of a metal reflector, artificial magnetic conductor (AMC) surface is proposed and applied on the reflector [10–15]. By setting AMC material between the antenna radiation arm and the metal ground, the antenna height is greatly reduced, and the antenna can maintain stable radiation patterns in the working frequency band. However, due to the narrow band of AMC material, the bandwidth of this kind of antenna is generally narrow. In addition, the antenna structure will be more complex and slightly bulky when AMC material is loaded.

In order to solve the mentioned problems, a square ring loaded ±45° dual polarization antenna unit is proposed. Based on the dual polarized rhombic antenna unit, the working bandwidth of the antenna unit is effectively broadened, and the antenna profile is reduced by loading a metal square ring under the rhombic patch and designing multi-section impedance transformation section. The square ring loaded on the antenna can make the working frequency of the antenna expand to low frequency, so as to reduce the antenna profile. In the frequency band of 2.4–3.8 GHz (relative bandwidth 45.1%), the VSWR of the antenna unit is less than 1.4, and the port isolation is greater than 27 dB. The maximum gain of main polarization is above 8.8 dBi, and the cross-polarization ratio of main polarization is more than 16 dB. On the basis of the designed antenna unit, a 2-element dual polarization array is designed, and the corresponding power division feed network is also designed. In order to ensure the stability of

Received 29 April 2021, Accepted 25 June 2021, Scheduled 5 August 2021
* Corresponding author: Wenkai Xu (648128448@qq.com).
The authors are with the Department of Communication Engineering, Nanjing University of Science and Technology, Nanjing 210094, China.

the horizontal pattern of the antenna in the frequency band, metal baffles are loaded on both sides of the antenna unit. In the range of 2.4–3.8 GHz, the VSWR of the 2-element array is less than 1.5, and the azimuth beam width is stable in the range of $60° \pm 5°$. In this paper, the designed antenna array is fabricated and tested. The measurement and simulation results show that the proposed antenna has practical application value in 5G micro base station system.

This paper is organized as follows. In Section 2, a dual polarization antenna unit is simulated and discussed. Based on the designed antenna unit, a 2-element antenna array is simulated and designed. Then, in Section 3, the designed antenna array is fabricated and tested, and the comparison of the measurement results with the simulation results is done. Finally, the conclusion of this work is drawn in Section 4.

2. ANTENNA DESIGN

2.1. Antenna Unit Structure

The geometry of the proposed antenna is shown in Figure 1. The antenna is divided into a radiation module, a feed module, and a metal reflector from top to bottom. The radiation module is located at the top. The feed module is composed of two orthogonal printed boards, which feed the two polarized radiation modules respectively, support the radiation module above, and connect with the reflector.

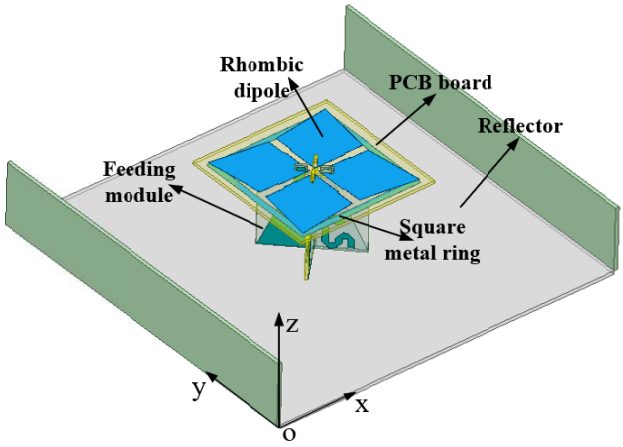

Figure 1. Geometry of the proposed antenna.

The structure of the antenna radiation module is shown in Figure 2. The yellow part is PCB, and the blue part is metal copper. The top layer of the radiation module PCB is composed of two pairs of rhombic dipoles, which are placed in the form of $\pm 45°$ dual polarization dipoles, and the bottom layer of the PCB is a square metal ring. The bottom metal ring can resonate at low frequency, so as to improve the impedance matching of antenna at low frequency. The central part of the radiation module PCB is provided with four slots which are connected with the lower feeding module. In order to further expand the working bandwidth of the antenna, the slot between each pair of dipoles has a step shape. The PCB used in the antenna radiation module is FR4 material (dielectric constant is 4.4, and loss tangent is 0.02), and the thickness is 0.8 mm.

The feeding part is shown in Figure 3. The feeding structure of each pair of dipoles is divided into two sides. One side of the feed printed circuit board (PCB) connector has multiple transmission lines on the front, and the other side is copper clad with trapezoidal progressive shape. The feed PCB is slotted in the middle to facilitate the splicing and combination of two orthogonal pieces. The trapezoidal structure on the back of each printed board of the feed module is a balun structure, which is used to adjust the balanced feed and improve antenna impedance matching with transmission lines. The trapezoidal structure facilitates the transition of feeding ports between the feeding network and the radiation part. The dielectric constant of the PCB in this part is 2.97; the tangent value of loss angle

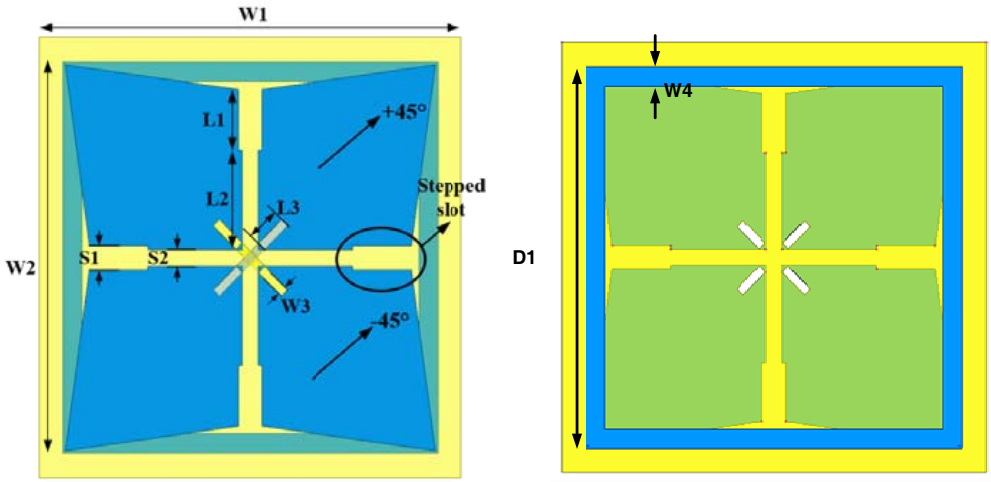

Figure 2. Geometry of the antenna radiation module. (a) Top view. (b) Back view.

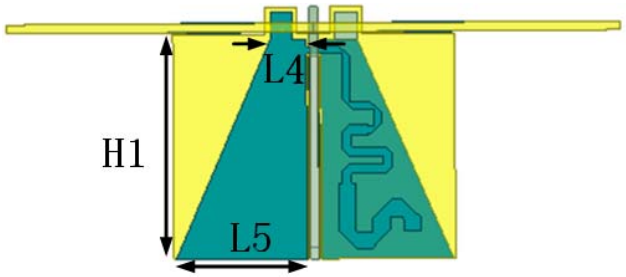

Figure 3. Geometry of the antenna feeding part.

Table 1. Parameters of the proposed antenna.

Parameter	Value (mm)	Parameter	Value (mm)	Parameter	Value (mm)
$W1$	40	$S1$	2.2	$L3$	3.0
$W2$	35	$S2$	1.5	$L4$	3.3
$W3$	35.5	$L1$	5.5	$L5$	12.1
$W4$	1.8	$L2$	9.0	$H1$	20.8

is 0.002; and the thickness is 0.762 mm. The dimensions of each structure of the antenna are shown in Table 1. The profile height is 20.8 mm, which is less than one quarter of the wavelength (24.2 mm) of the central frequency point ($f = 3.1$ GHz) and has low profile characteristics. The feed PCB is different from the radiation module PCB. Feed PCB has lower loss tangent than the radiation module PCB in order to reduce the RF loss.

2.2. Performance and Analysis of Antenna Unit

In order to distinguish two pairs of dipoles, the two pairs are named as $+45°$ polarized dipole and $-45°$ polarized dipole, respectively, as shown in Figure 2(a). The VSWR and isolation degree of the antenna unit are shown in Figure 4 and Figure 5, respectively. It can be seen from the figure that the $\pm 45°$ dipole port of antenna unit is within the whole frequency range of 2.4–3.8 GHz, and the VSWR is below

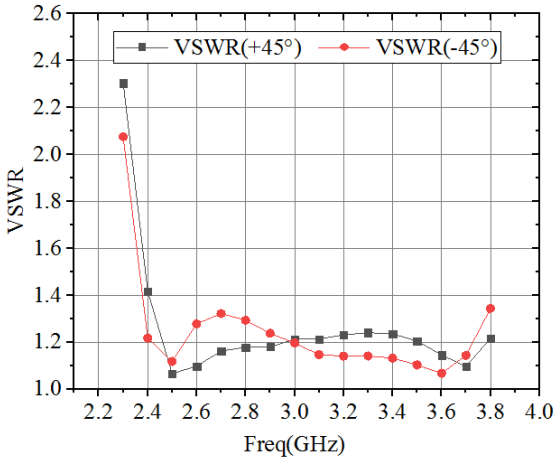

Figure 4. VSWRs of the antenna unit.

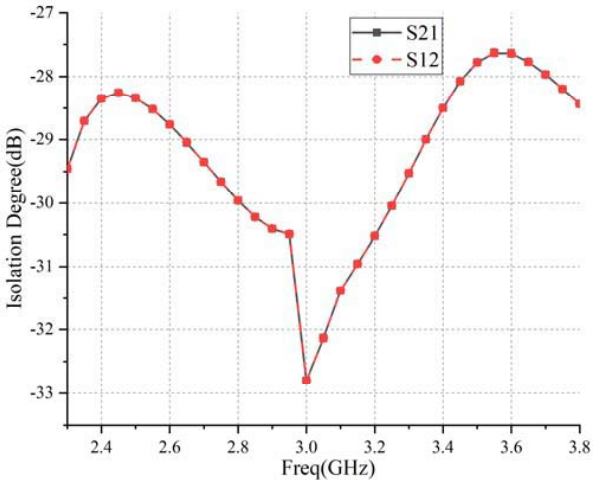

Figure 5. Isolation degrees of the antenna unit.

1.4. In the working band, the VSWR of the +45° polarize dipole is less than 1.3 in the 2.5–3.8 GHz, and the VSWR of the −45° polarized dipole is slightly higher in the frequency band of 2.6–2.8 GHz. The isolation between the two ports is less than −27 dB in the full band, and the isolation degree in the 2.2–3.5 GHz band is less than −28 dB, which indicates that the coupling between the two ports of the antenna is low and meets the industrial requirements. Due to the symmetrical structure of the ±45° dipoles and similar S-parameter values, the performance of the −45° polarized antenna is only discussed later in this paper.

The VSWRs of antenna before and after adding metal square ring are shown in Figure 6. It can be seen that the low-frequency bandwidth is expanded after adding the metal ring. The original antenna only achieves the VSWR below 1.5 in the bandwidth of 3.4–3.8 GHz. While the antenna unit loaded with a square ring can work in the frequency band of 2.4–3.8 GHz, the VSWR is less than 1.4. After adding the square ring, the surface currents of low, medium, and high frequency points of the antenna are shown in Figure 7. The current distribution when the antenna is not loaded with a square ring is also shown in Figure 8 for comparison.

It can be seen from Figure 7 that when the antenna is working at low frequency (2.8 GHz), the surface current of the two antennas is mainly concentrated in the metal ring region at the tip of the −45° polarized rhombic oscillator and its corresponding position, which indicates that there is resonance

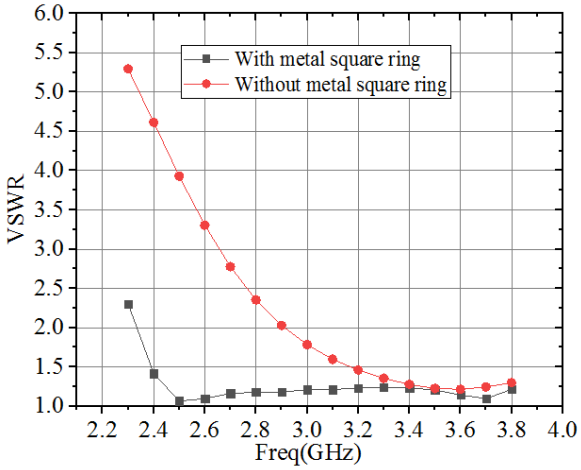

Figure 6. VSWRs before and after ring addition.

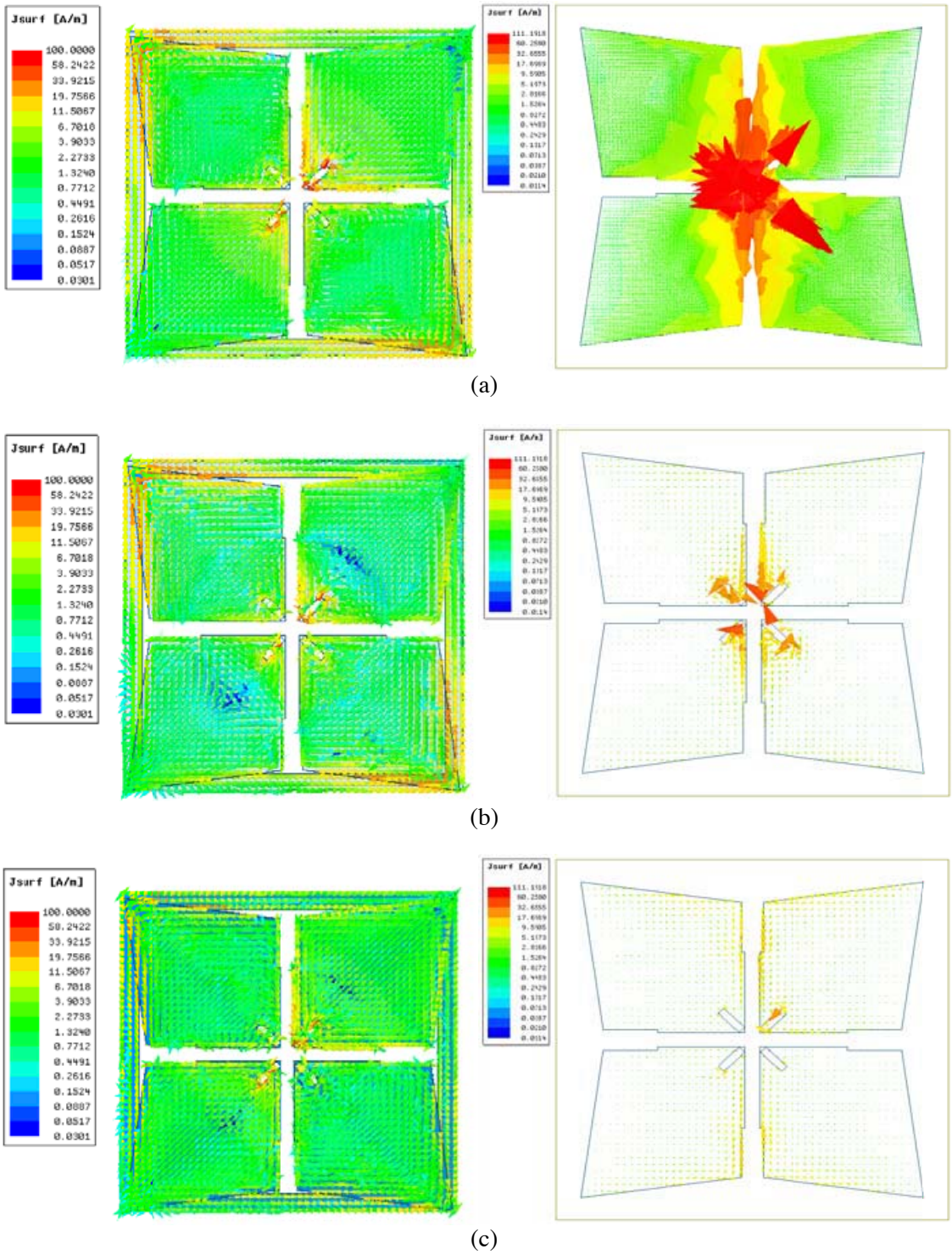

Figure 7. Surface current distributions with and without a square ring at low, medium and high frequency points. (a) 2.8 GHz, (b) 3.3 GHz, (c) 3.8 GHz.

between the metal ring and the oscillator. The magnitudes of the surface currents of the two antennas are similar, and the energy is radiated by the dipole and metal ring together. Compared with the low frequency (2.8 GHz), when the antenna works in the medium frequency (3.3 GHz), the concentrated

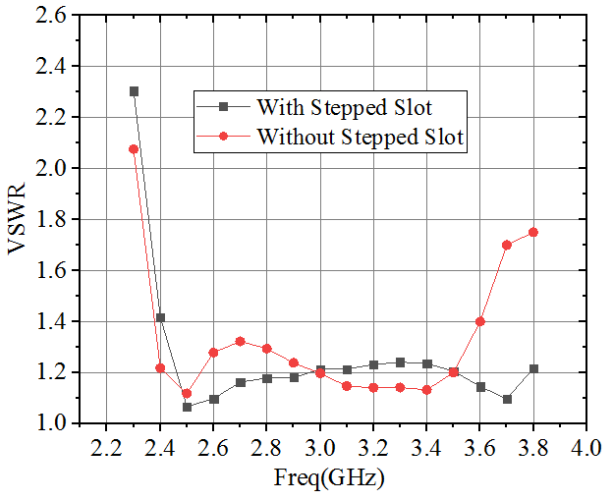

Figure 8. VSWRs before and after stepped slot addition.

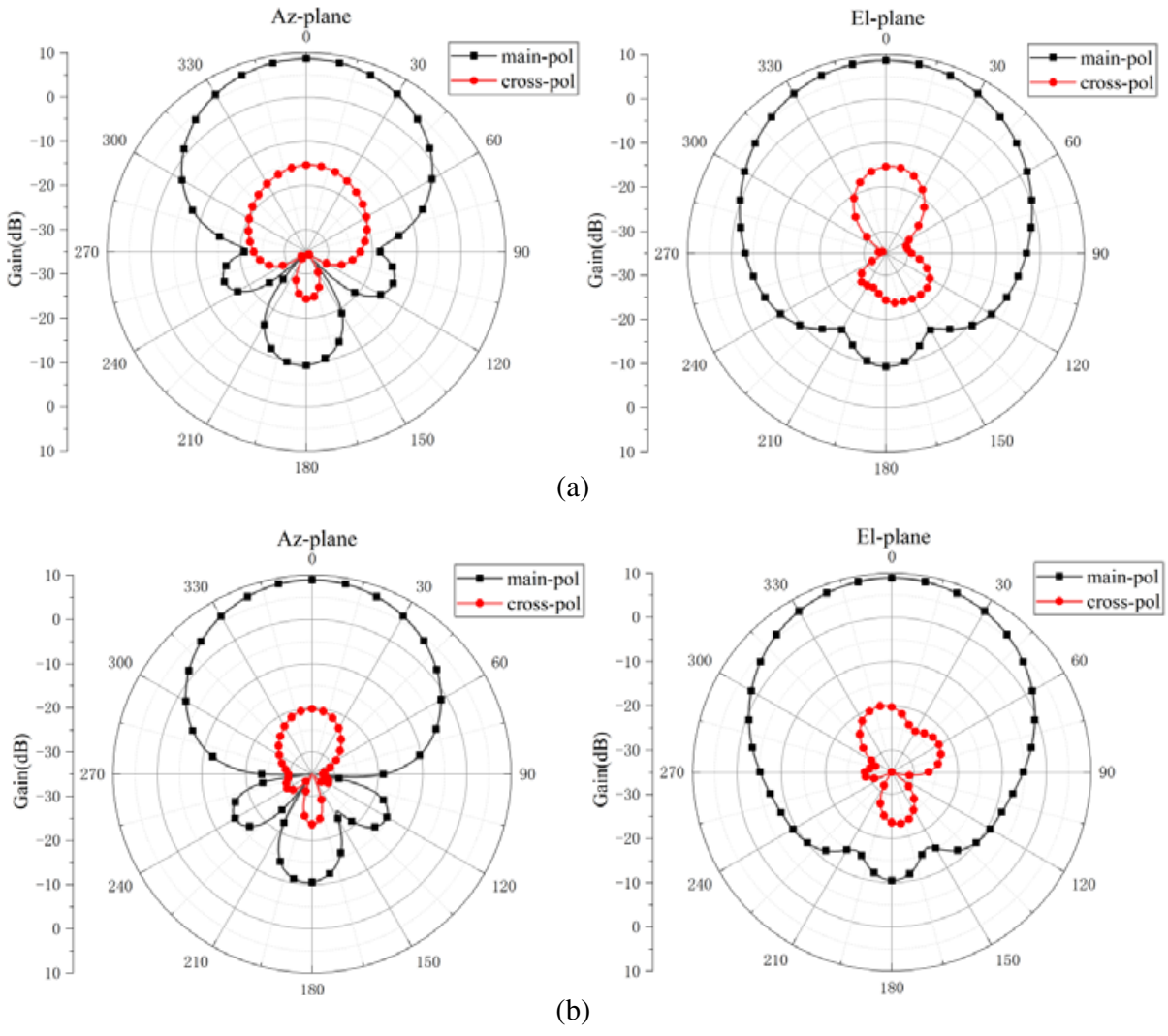

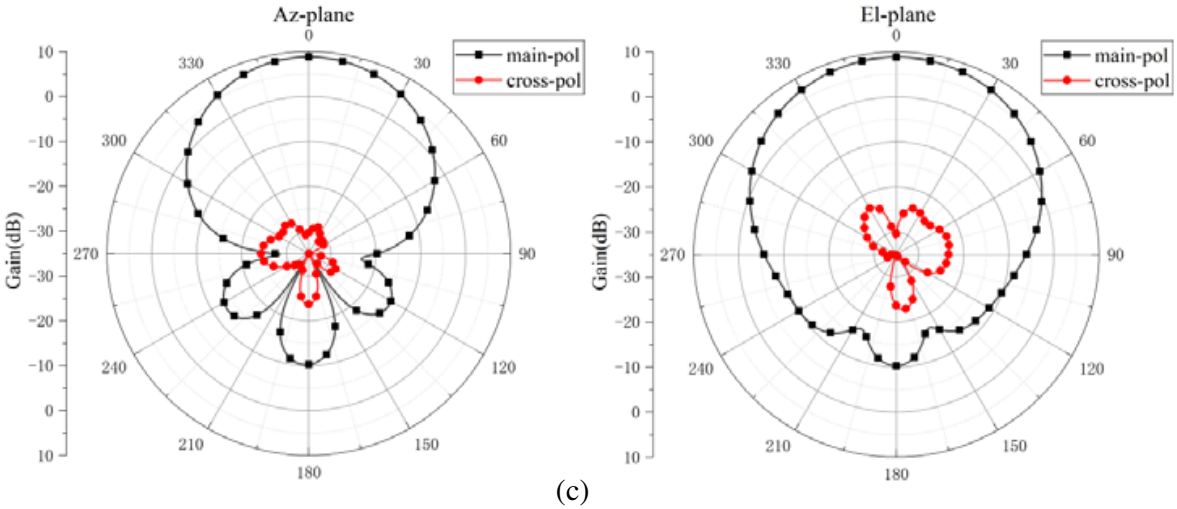

(c)

Figure 9. Antenna patterns of low, medium, and high frequency points. (a) 2.8 GHz, (b) 3.3 GHz, (c) 3.8 GHz.

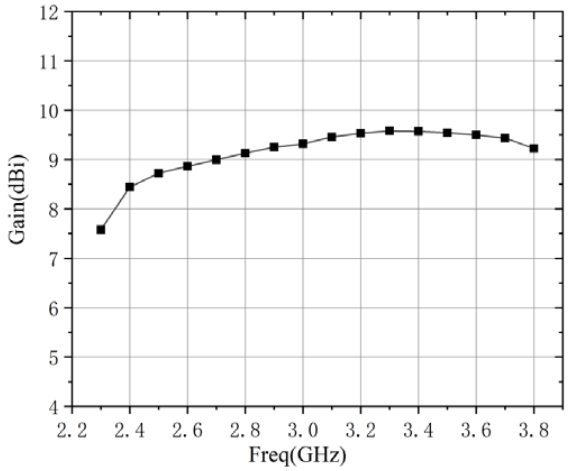

Figure 10. Diagram of max antenna unit gain vs frequency band.

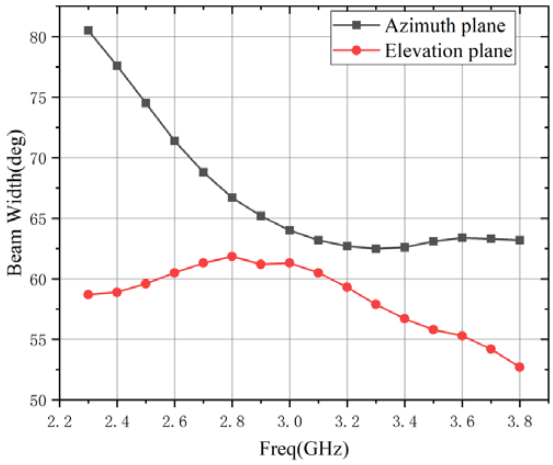

Figure 11. Diagram of antenna unit beam width vs frequency band.

position of the surface current moves to both sides of the tip of the dipole, and the magnitudes of the surface currents are the same at the edge of the dipole and the corresponding metal ring region. When working at high frequency (3.8 GHz), the surface current is mainly distributed on the arm near the feed port, and the surface current is significantly reduced compared with that at low frequency (2.8 GHz) and medium frequency (3.3 GHz). This phenomenon shows that when the antenna works at medium and low frequency (2.4–3.3 GHz), the metal ring will resonate with the dipole, which improves the radiation performance of the antenna in this frequency band. The variation trend of surface current of antenna at high, medium, and low frequencies is consistent with the difference VSWR before and after adding metal ring in Figure 6, which indicates the effectiveness of adding a metal ring to expand low frequency bandwidth.

Inspired by the influence of the square metal ring loading on the current, each pair of dipole arms near the feeding part is modified into a stepped slot structure, so as to change the surface current at high frequency. The comparison of VSWR with or without a stepped slot is shown in Figure 8. After adding a stepped slot, the VSWR of the antenna at 3.5–3.8 GHz is obviously better than that before, and the high frequency cut-off frequency is expanded to 3.8 GHz.

The patterns of low, medium, and high frequency points are shown in Figure 9. The azimuth plane is XOZ plane, and the elevation plane is YOZ plane. The frequency of the maximum gain of the antenna unit changing with frequency is shown in Figure 10, and the beam widths of the azimuth plane and elevation plane of the antenna unit changing with frequency are shown in Figure 11. It can be seen from these figures that the maximum gain of the antenna increases gradually from the low frequency 2.6 GHz to the 3.3 GHz frequency point. When the gain of 3.3 GHz frequency point reaches the peak value, the gain begins to decrease with the increase of frequency. This phenomenon is consistent with the fact that the surface current of 3.8 GHz frequency point is lower than that of 3.3 GHz frequency point, which indicates that the antenna impedance mismatch is obvious, and the radiation efficiency is reduced. The main polarization cross polarization ratio is 19 dB at low frequency (2.8 GHz) and 16 dB at high frequency (3.8 GHz) in the normal direction of the antenna pattern.

2.3. Antenna Array Design

Based on the antenna elements in the previous section, a 2-element antenna array is formed using the two elements as one column. As shown in Figure 12, each column of antenna dipoles with the same polarization is fed with a 1 : 2 power divider. The 1 : 2 power divider has chosen the form of a branch line structure to save space. There are baffles on the left and right sides of each antenna column, and each baffle has the same horizontal spacing as the antenna. In addition, a central adjustment baffle is added between two antenna arrays to adjust the beamwidth. The structure dimensions of the antenna array and power divider are shown in Table 2.

Table 2. Some parameters of the antenna array and 1 : 2 power divider.

Parameter	Value (mm)
$D1$	95
$L1$	180
$W1$	90
$W2$	20
$W3$	2
$W4$	0.6

The isolation degree of the two ports in each column of the antenna array is shown in Figure 13, and the VSWRs are shown in Figure 14. It can be seen from the figure that the isolation between ports in the full band is below -22 dB, and the VSWR is less than 1.5.

To study the effect of the central control plate on the antenna, only one column is fed here, and the other is connected with a matching load. The azimuth and elevation patterns before and after adding intermediate adjustment baffle are shown in Figure 15, and the beam width varying with frequency is shown in Figure 16. The comparison shows that the central adjustment baffle has little effect on the elevation pattern. For the azimuth plane, the central control plate narrows the beam width. As a result, the radiation energy is more concentrated when a central baffle is added.

3. MANUFACTURING AND MEASUREMENT

In order to verify the performance of the antenna, the 2-element array is processed. The fabricated antenna array and radome are shown in Figure 17. The Grey bottom plate is an aluminum plate. In order to facilitate the adjustment and obtain better performance effect, the baffle plate between the two groups of binary antennas is made of a copper sheet, and two groups of baffle plates are also added in the elevation direction.

The Keysight technologies E5071C is used to test the isolation between the two ports of each antenna unit and VSWRs of the two ports of each unit. The antenna pattern is tested in a small far field. The comparison between the actual test and simulation results of the VSWR of Port 1 is shown

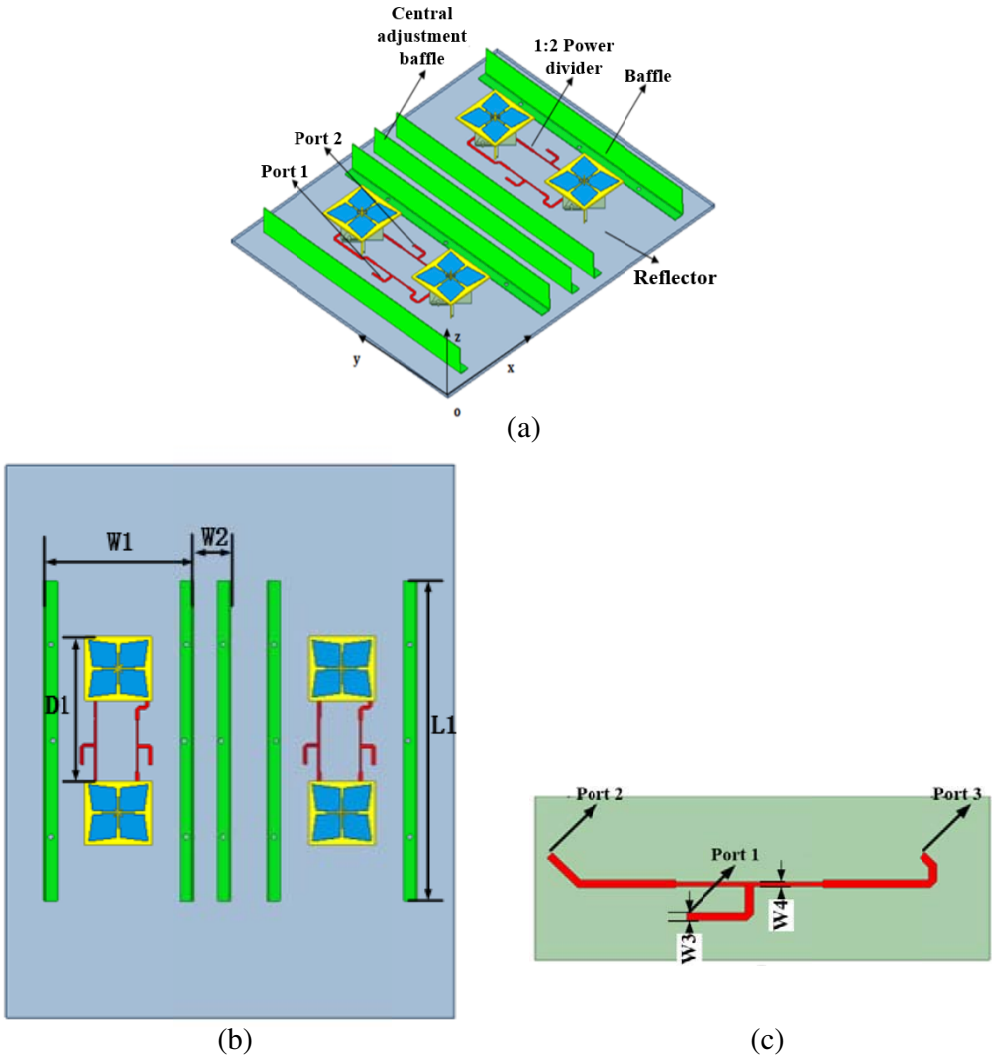

Figure 12. Diagram of 2-element binary array. (a) Overall structure diagram. (b) Top view. (c) 1 : 2 power divider structure.

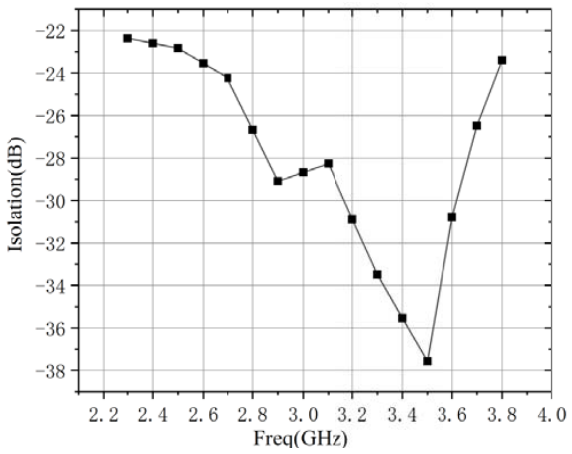

Figure 13. Isolation degree between two antenna ports.

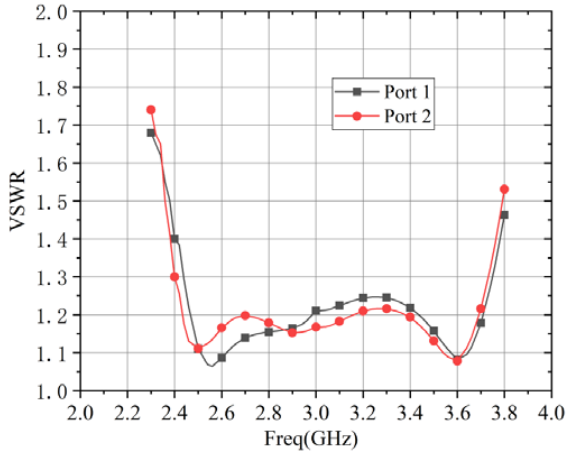

Figure 14. VSWR of two antenna ports.

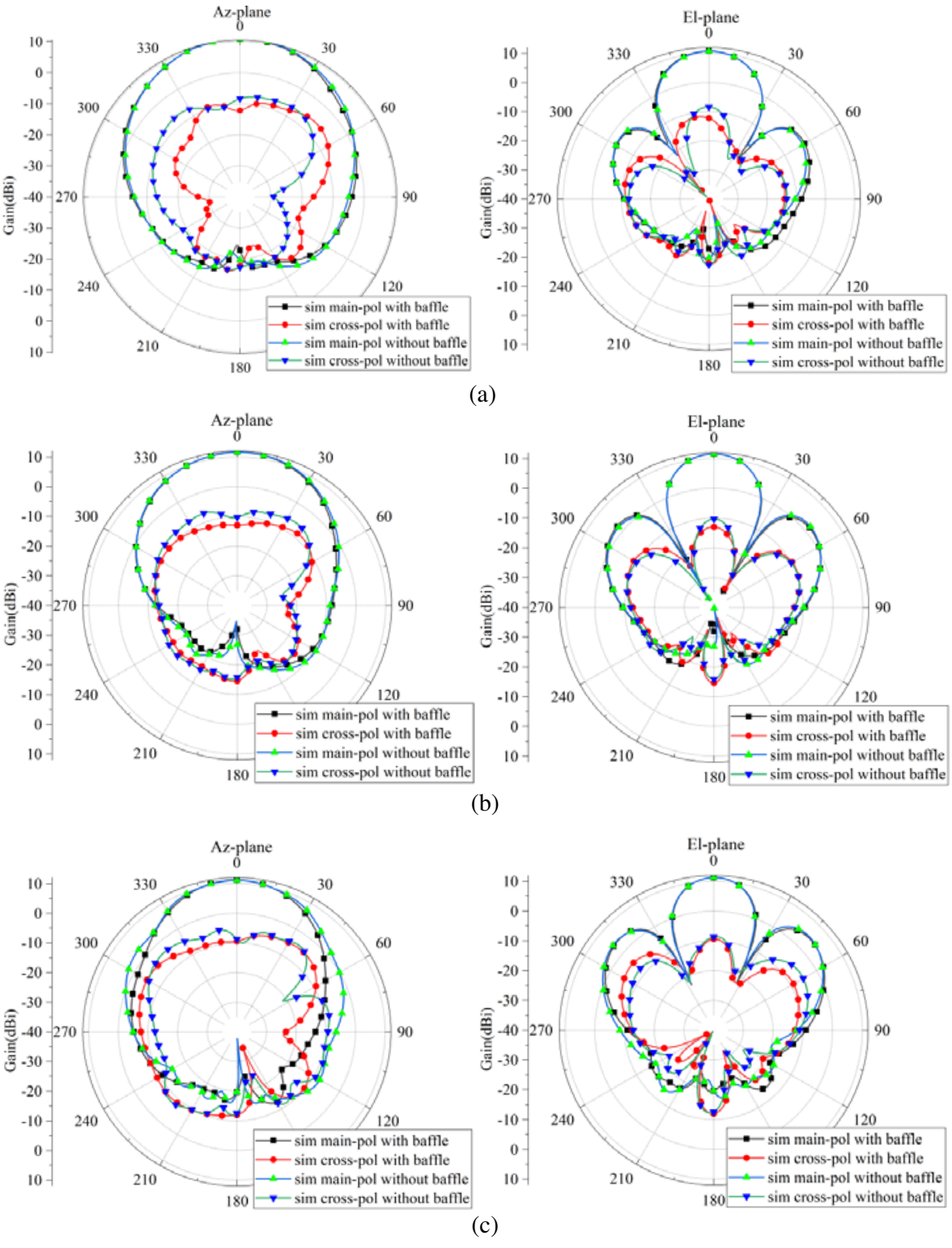

Figure 15. Antenna pattern before and after loading intermediate adjustment baffle. (a) 2.8 GHz, (b) 3.3 GHz, (c) 3.8 GHz.

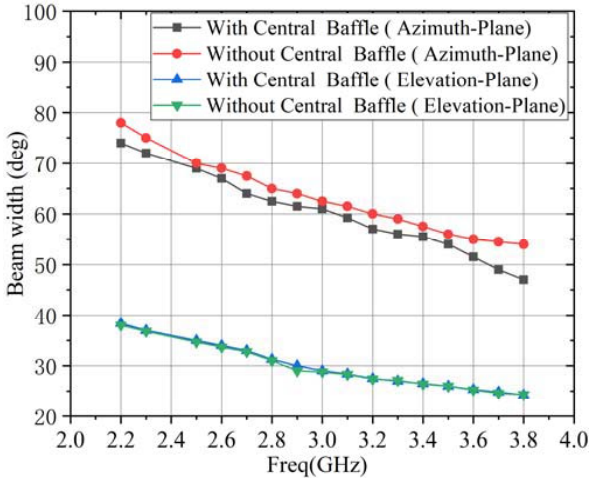

Figure 16. Beam width versus frequency.

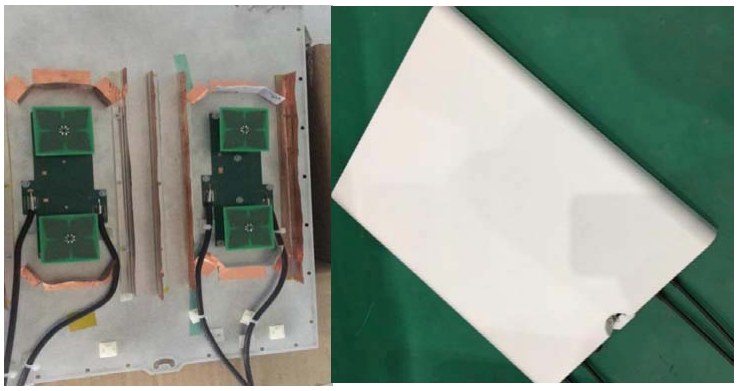

(a) (b)

Figure 17. The photograph of the fabricated antenna array. (a) Fabricated antenna array. (b) The diagram of the antenna radome.

in Figure 18, and the comparison between the measured and simulated results of isolation between two ports in the same unit are shown in Figure 19. It can be seen from these figures that the test results are in good agreement with the simulation ones.

The comparison between the measured pattern and simulated pattern is shown in Figure 20. It can be seen from the figure that the measured pattern is consistent with the simulated one. Due to the influence of feeding and microwave anechoic chamber environment, there are some deviations between the measured and simulated results. The performance of the proposed antenna compared with other Dual-Polarized Low-Profile antennas is given in Table 3.

Table 3. Comparison between proposed and previous works.

Ref.	Bandwidth (GHz)	Height (mm)	HPBW (deg)
[6]	1.7–2.7 (45%)	33	66.5 ± 3.5
[9]	0.79–0.96 (19%)	74	65 ± 5
[11]	2.4–2.7 (12%)	17	67 ± 1
This Work	2.4–3.8 (45.16%)	20.8	69.5 ± 5.5

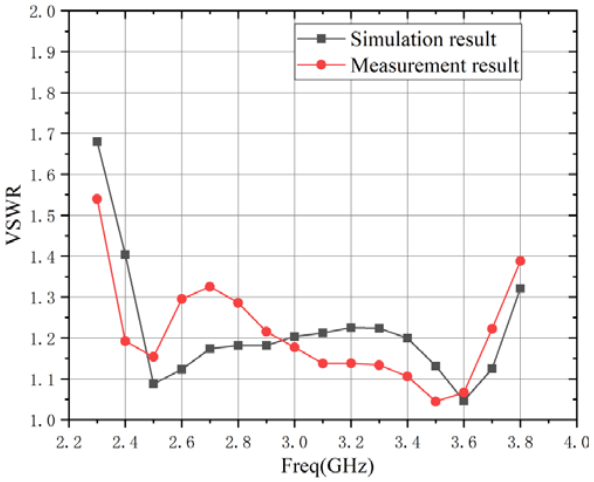

Figure 18. Comparison of measured and simulated VSWR results of Port 1.

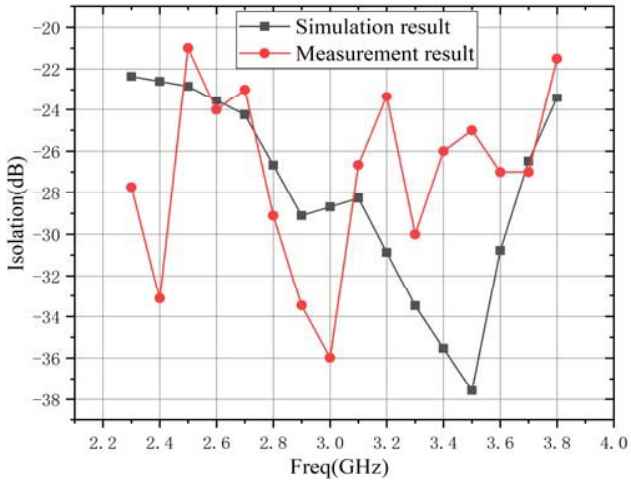

Figure 19. Comparison of measured and simulated results of the isolation between two ports in the same unit.

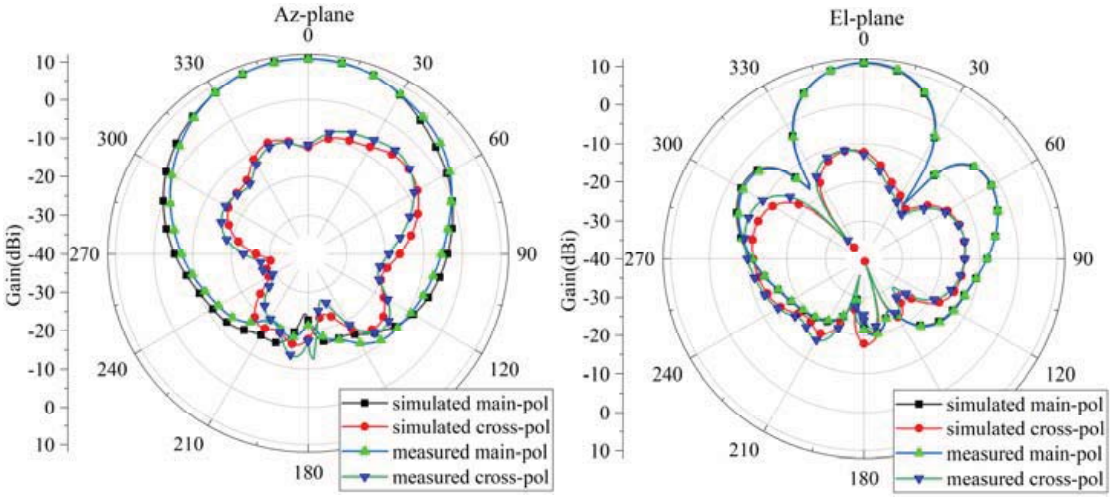

(a)

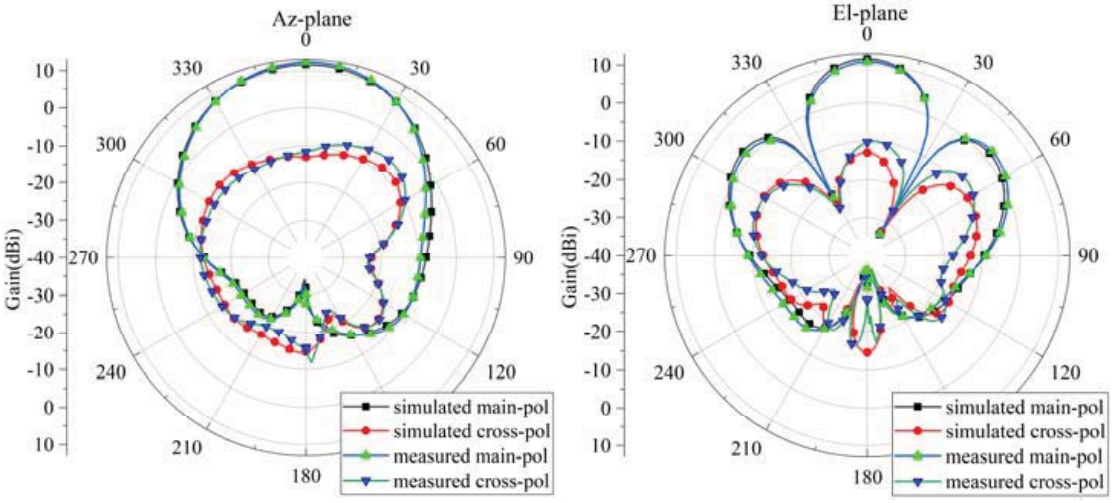

(b)

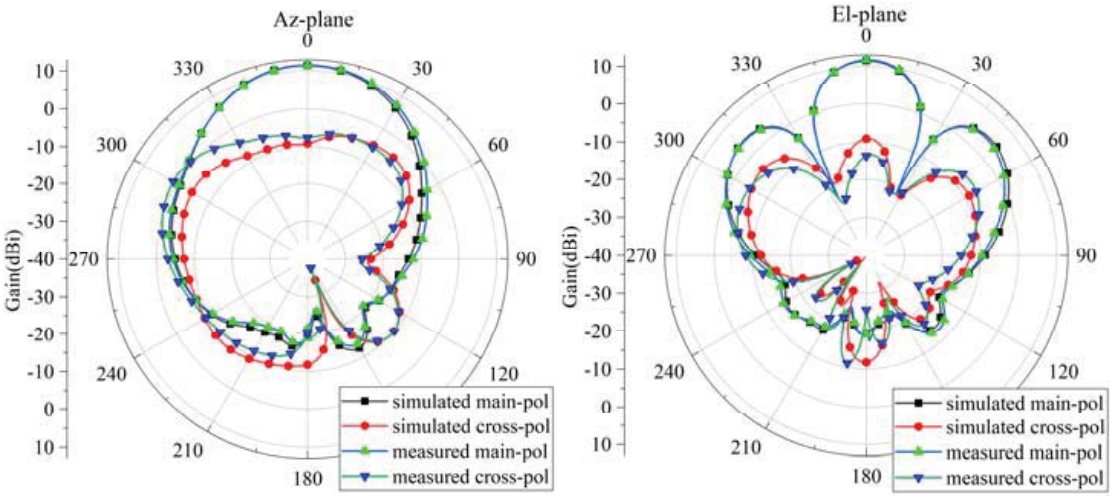

(c)

Figure 20. Comparison of array measured and simulated pattern. (a) 2.8 GHz, (b) 3.3 GHz, (c) 3.8 GHz.

By comparison, it can be seen that the antenna elements described in this paper have the characteristics of low profile, wide bandwidth, and wide bandwidth.

4. CONCLUSION

In this paper, a low-profile antenna unit is designed by the loading of a metal ring and the changing of dipole arms. The VSWR is less than 1.4 in the frequency band of 2.4–3.8 GHz, and the gain of each pair of dipoles is between 8.6 and 9.6 dBi. The reason of expanding bandwidth by loading metal ring is analyzed from the perspective of surface current. Based on the antenna unit, a 2-element array is designed. Besides, an additional metal baffle is added in the center of the array to reduce the mutual coupling between antenna elements. Finally, the 2-element array is fabricated, and the S parameters and pattern are measured. The experimental results are consistent with the simulation ones, which also meet the actual industrial needs. The proposed antenna has practical application value in 5G micro base station system.

REFERENCES

1. Liang, Z., C. Lu, Y. Li, J. Liu, and Y. Long, "A broadband dual-polarized antenna with front-to-back ratio enhancement using semi cylindrical sidewalls," *IEEE Trans. Antennas Propag.*, Vol. 66, No. 7, 3735–3740, Jul. 2018.
2. Cui, Y., R. Li, and H. Fu, "A broadband dual-polarized planar antenna for 2G/3G/LTE base stations," *IEEE Trans. Antennas Propag.*, Vol. 62, No. 9, 4836–4840, Sep. 2014.
3. Li, M. and K. M. Luk, "Wideband magnetoelectric dipole antennas with dual polarization and circular polarization," *IEEE Antennas Propag. Mag.*, Vol. 57, No. 1, 110–119, Feb. 2015.
4. Zhang, Q. and Y. Gao, "A compact broadband dual-polarized antenna array for base stations," *IEEE Antennas Wireless Propag. Lett.*, Vol. 17, No. 6, 1073–1076, Jun. 2018.
5. He, Y., Z. Pan, X. Cheng, Y. He, J. Qiao, and M. M. Tentzeris, "A novel dual-band, dual-polarized, miniaturized and low-profile base station antenna," *IEEE Trans. Antennas Propag.*, Vol. 63, No. 12, 5399–5408, Dec. 2015.
6. Ding, C., H. Sun, R. W. Ziolkowski, and Y. J. Guo, "A dual layered loop array antenna for base stations with enhanced cross-polarization discrimination," *IEEE Trans. Antennas Propag.*, Vol. 66, No. 12, 6975–6985, Dec. 2018.

7. Qin, P., L. Ji, S. Chen, and Y. J. Guo, "Dual-polarized wideband Fabry-Perot antenna with quad-layer partially reflective surface," *IEEE Antennas Wireless Propag. Lett.*, Vol. 17, No. 4, 551–554, Apr. 2018.
8. Huang, H., Y. Liu, and S. Gong, "A dual-broadband, dual-polarized base station antenna for 2G/3G/4G applications," *IEEE Antennas Wireless Propag. Lett.*, Vol. 16, 1111–1114, Nov. 2016.
9. He, Y., W. Tian, and L. Zhang, "A novel dual-broadband dual-polarized electrical downtilt base station antenna for 2G/3G applications," *IEEE Access*, Vol. 5, 15241–15249, 2017.
10. Chu, Q. X., D. Wen, and Y. Luo, "A broadband $\pm 45^{\circ}$ dual-polarized antenna with Y-shaped feeding lines," *IEEE Trans. Antennas Propag.*, Vol. 63, 483–490, Feb. 2015.
11. Liu, Y., J. Wang, and S. Gong, "Low-profile dual-polarized planar antenna with compact structure for base stations," *Chin. J. Electron.*, Vol. 26, 1092–1095, 2017.
12. Zhai, H., K. Zhang, S. Yang, and D. Feng, "A low-profile dual-band dual-polarized antenna with an AMC surface for WLAN applications," *IEEE Antennas Wireless Propag. Lett.*, Vol. 16, 2692–2695, 2017.
13. Li, M., Q. L. Li, B. Wang, C. F. Zhou, and S. W. Cheung, "A low profile dual-polarized dipole antenna using wideband AMC reflector," *IEEE Trans. Antennas Propag.*, Vol. 66, No. 5, 2610–2615, May 2018.
14. Feresidis, A. P., G. Goussetis, S. Wang, and J. C. Vardaxoglou, "Artificial magnetic conductor surfaces and their application to low-profile high-gain planar antennas," *IEEE Trans. Antennas Propag.*, Vol. 53, No. 1, 209–215, Jan. 2005.
15. Li, M., K. M. Luk, L. Ge, and K. Zhang, "Miniaturization of magnetoelectric dipole antenna by using metamaterial loading," *IEEE Trans. Antennas Propag.*, Vol. 64, No. 11, 4914–4918, Nov. 2016.